Author(s): Lipiäinen, Lauri & Kokkonen, Kimmo & Kaivola, Matti

Title: Phase sensitive absolute amplitude detection of surface vibrations using homodyne interferometry without active stabilization

Year: 2010

Version: Final published version

Please cite the original version:

Lipiäinen, Lauri & Kokkonen, Kimmo & Kaivola, Matti. 2010. Phase sensitive absolute amplitude detection of surface vibrations using homodyne interferometry without active stabilization. Journal of Applied Physics. Volume 108, Issue 11. 114510. ISSN 1089-7550 (electronic). ISSN 0021-8979 (printed). DOI: 10.1063/1.3504636.

AIP Journal of Applied Physics

Phase sensitive absolute amplitude detection of surface vibrations using homodyne interferometry without active stabilization

Lauri Lipiäinen, Kimmo Kokkonen, and Matti Kaivola

Citation: Journal of Applied Physics **108**, 114510 (2010); doi: 10.1063/1.3504636
View online: http://dx.doi.org/10.1063/1.3504636
View Table of Contents: http://scitation.aip.org/content/aip/journal/jap/108/11?ver=pdfcov
Published by the AIP Publishing

Phase sensitive absolute amplitude detection of surface vibrations using homodyne interferometry without active stabilization

Lauri Lipiäinen,[a] Kimmo Kokkonen, and Matti Kaivola
Department of Applied Physics, Aalto University School of Science and Technology, P.O. Box 13500, 00076 Aalto, Finland

(Received 23 June 2010; accepted 21 September 2010; published online 10 December 2010)

A detection scheme for obtaining phase and absolute amplitude information of surface vibrations on microacoustic components using homodyne laser interferometry is described. The scheme does not require active stabilization of the optical path length of the interferometer. The detection setup is realized in a homodyne Michelson interferometer configuration, and selected measurements on a 374 MHz surface acoustic wave fan-shaped filter and two different piezoelectrically actuated micromechanical resonators are presented to demonstrate the performance of the instrument. With the current detection electronics, the interferometer is capable of detecting out-of-plane surface vibrations up to 2 GHz with a lateral resolution of better than 1 μm and with a minimum detectable vibration amplitude of ~1 pm. © *2010 American Institute of Physics*. [doi:10.1063/1.3504636]

I. INTRODUCTION

A multitude of microacoustic components have been introduced for large-scale commercial applications during the last few decades. For example, high-performance, low-loss radio frequency filters based on surface acoustic wave (SAW), and bulk acoustic wave technologies are now widely used in wireless communication systems. Also microelectromechanical (MEMS) resonators have been under growing research interest. MEMS resonators are considered, e.g., as potential replacements for discrete quartz crystals in timing and frequency control applications with additional benefits such as compact size, low power consumption, and integrability to silicon circuits. As the operation of microacoustic components is based on mechanical vibrations, it is important to be able to study the vibration fields directly to better understand the underlying physics, and hence, to improve the device design. As a noncontact method, laser interferometry has proven to be a useful tool for characterizing surface vibrations of these components (see, e.g., Refs. 1–7).

For a quantitative characterization of microacoustic components, interferometric measurements should preferably provide phase and absolute amplitude information of the vibration fields. Such data allow for, e.g., separation of waves propagating into different directions, analysis of acoustic reflections, and determination of dispersion properties. In addition, the surface movements may be animated to visualize the dynamics of the vibration fields in slow motion.

Heterodyne interferometry and stabilized homodyne interferometry are the commonly used approaches for the detection of the phase and absolute amplitude of surface vibrations. In stabilized homodyne interferometry, the optical path length of the interferometer is actively controlled to stabilize the instrument to a quadrature point (QP).[8,9] Such stabilization is not needed in heterodyne interferometers, which utilize an optical frequency shift between the interfering beams and a two-frequency detection technique.[5,6]

In this work, a laser-interferometric method for phase-sensitive absolute amplitude detection of surface vibrations using homodyne technique is presented. The detection scheme does not require active optical path stabilization. Hence, the method allows for an interferometer design with no feedback loop control of the optical path length or optical heterodyning. In the detection setup described here, the optical path length of the reference beam is swept at each measurement point such that the operation point of the interferometer is translated over several QPs. The intensity of the interference signal is recorded during the sweep as a function of the optical path length, and the phase and absolute amplitude data of the surface vibrations are then determined from the measured data.

The detection method is implemented in a scanning homodyne Michelson interferometer[10] configuration. It should however be noted that the method is more general and not restricted only to that interferometer type. To demonstrate the performance at different frequency ranges, the amplitude and phase fields of selected vibration modes in two piezoelectrically actuated MEMS resonators (10–60 MHz) and a fan-shaped SAW filter (374 MHz) are presented.

II. DETECTION PRINCIPLE

In the Michelson interferometer setup illustrated in Fig. 1, a polarizing beam splitter (PBS) divides the linearly polarized, collimated laser beam into sample and reference beams. The sample beam is focused onto the sample surface and reflected back. The reference beam propagates a similar distance to the reference mirror and back. The two beams are then combined at the PBS, after which they collinearly propagate through the analyzer resulting in an interference signal at the photodetector (PD). Assuming a sinusoidal vibration perpendicular to the sample surface, the time-dependent part of the intensity of the interference signal is of the form[11,12]

[a]Electronic mail: lauri.lipiainen@tkk.fi.

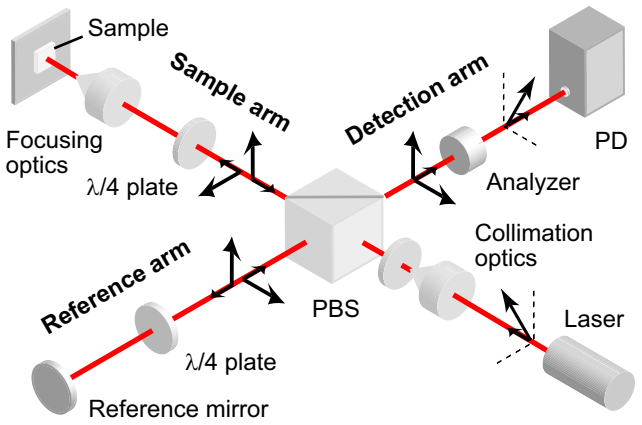

FIG. 1. (Color online) Schematic presentation of a homodyne Michelson interferometer for measuring surface vibrations. Black arrows indicate the propagation directions and linear polarization states of the beams. The λ/4 plates are used to rotate the polarization of the back-reflected beams such that the PBS will direct the beams to the detection arm. The analyzer enables the orthogonally polarized sample and reference beams to interfere on the PD.

$$I_t(t) = C\cos\left[\phi - \frac{4\pi}{\lambda} z\sin(2\pi f_{\mathrm{vib}} t + \Phi_{\mathrm{vib}})\right], \tag{1}$$

where the coefficient C is related, e.g., to the intensities of the two interfering beams, λ is the optical wavelength, z the amplitude of the vibration, f_{vib} and Φ_{vib} are the frequency and phase of the surface vibration, respectively, and ϕ is the optical phase difference between the sample and reference beams. The phase ϕ typically varies slowly ($\ll 10$ Hz) due to, e.g., variations in the ambient conditions. The surface vibrations of interest are assumed to be at higher frequencies ($f_{\mathrm{vib}} \gg 1$ kHz) than the changes in ϕ.

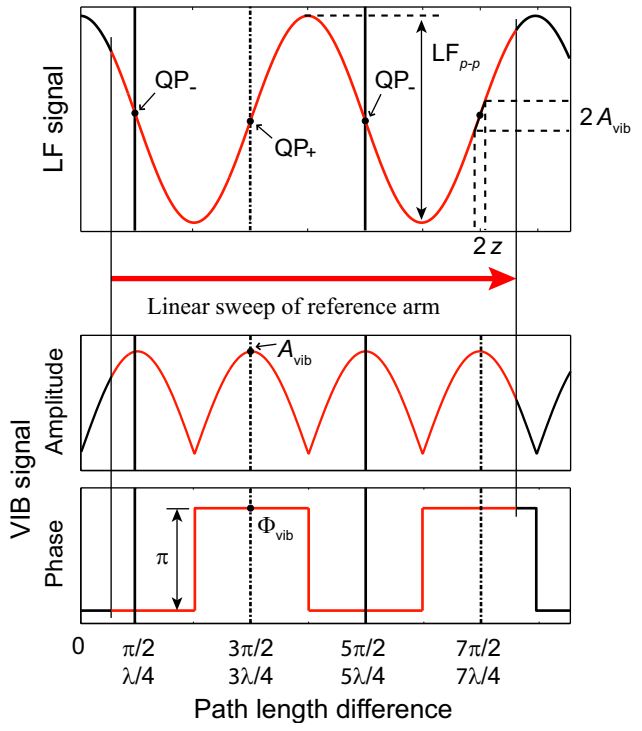

FIG. 2. (Color online) Qualitative illustration of the LF term (top curve) and the VIB term (amplitude and phase at surface vibration frequency f_{vib}, middle and bottom curves, respectively) of Eq. (2) as a function of the optical path length difference (or phase difference ϕ) between the sample and reference beams. In stabilized homodyne intereferometers, ϕ is stabilized at a single quadrature point QP_+ (or QP_-) to obtain Φ_{vib} unambiguously and to have the maximum amplitude signal A_{vib}.

In order to study the frequency content of the interference signal, Eq. (1) may be expanded to a harmonic series with amplitudes given by Bessel functions of the first kind.[12] For the detection principle presented here, it is sufficient to consider only the two lowest order components of the series expansion. For vibration amplitudes $z \ll \lambda$, Eq. (1) may be further approximated as

$$I_t(t) \approx \underbrace{C\cos(\phi)}_{\mathrm{LF}} + \underbrace{\frac{4\pi C}{\lambda} z\sin(2\pi f_{vib} t + \Phi_{vib})\sin(\phi)}_{\mathrm{VIB}}. \tag{2}$$

The term LF is related to ϕ and hence varies if the optical path length difference changes. The second term denoted as VIB depends additionally on the surface vibration parameters z, f_{vib}, and Φ_{vib}. The behavior of these two terms is qualitatively illustrated in Fig. 2 as a function of ϕ, or equivalently, the optical path length difference between the two beams.

The values $\phi = (2n-1)\pi/2$ with integer n correspond to the so-called QPs, at which the amplitude of the VIB term oscillating at f_{vib} reaches its largest value $A_{\mathrm{vib}} = 4\pi C z/\lambda$. For small vibration amplitudes $z \ll \lambda$, the interferometer response is also highly linear at around the QPs. Consequently, homodyne interferometers are typically stabilized to operate at a single QP by actively controlling the optical phase of the reference beam. Another benefit of the stabilization is that it enables an unambiguous detection of Φ_{vib} (see Fig. 2). Furthermore, by observing the error signal of the feedback loop controlling the phase of the reference beam, the absolute amplitude of the surface vibration may be obtained via calibration.[9]

If a homodyne interferometer is not actively stabilized to a single QP, the amplitude and phase cannot be determined by merely measuring the VIB signal due to drifts in the optical path lengths of the sample and reference beams. In particular, the result of the phase measurement would have $\pm\pi$ rad shifts every time $\cos(\phi)$ drifts from a negative to a positive slope or vice versa, see Fig. 2.

To overcome these problems, a linear sweep of the optical path length is utilized in this detection scheme as illustrated in Fig. 2. During the sweep, both the high-frequency VIB signal and the low-frequency LF signal are simultaneously measured from the interference signal at each measurement point on the sample. To illustrate the behavior of the LF and VIB signals over several QPs, an optical path length sweep of the reference beam over a distance of $>3\lambda/2$ is shown in Fig. 2.

The QPs are located by finding the maximum slopes of the recorded LF signal. The amplitude A_{vib} of the surface vibration is then determined from the amplitude data of the VIB signal at the located QPs. In practical measurements, either a single amplitude value at a single QP may be used or an average of amplitude values at several QPs may be calculated to determine the vibration amplitude A_{vib} to be recorded. The LF signal also serves as a measure of the modu-

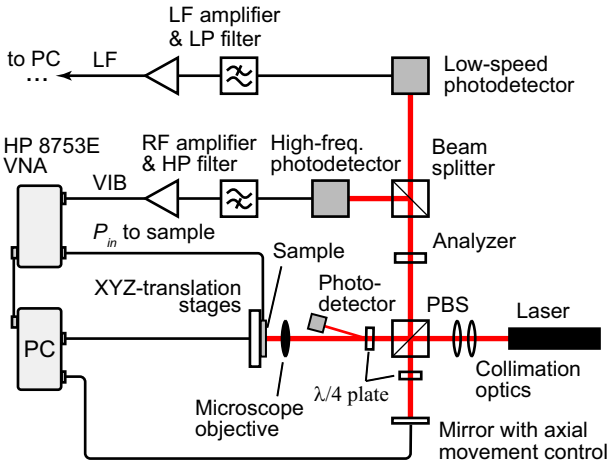

FIG. 3. (Color online) Schematic representation of the homodyne Michelson interferometer setup with phase and absolute amplitude detection. HP—high-pass, LP—low-pass.

lation depth of the interference which can be used to determine the absolute amplitude of the surface vibrations. By determining the peak-to-peak amplitude $\mathrm{LF}_{p-p}=2C$ of the LF signal, the detected amplitude maximum A_{vib} is found to be [see Eq. (2) and Fig. 2]

$$A_{\mathrm{vib}}=\frac{4\pi}{\lambda}Cz=\frac{4\pi}{\lambda}\frac{\mathrm{LF}_{p-p}}{2}z, \tag{3}$$

from which an absolute value for the vibration amplitude z may be calculated as

$$z=\frac{\lambda}{2\pi}\frac{A_{\mathrm{vib}}}{\mathrm{LF}_{p-p}}. \tag{4}$$

To obtain the phase of the vibration Φ_{vib} unambiguously, the slope type of the LF signal is identified at each QP (positive or negative slope, QP_+ or QP_-, respectively). The phase Φ_{vib} may be determined from the recorded phase data of the VIB signal by looking for QPs of the same type (negative or positive slope).

This phase-sensitive absolute amplitude detection may be implemented in multiple ways. The only necessary requirement is to carry out the sweep of the optical path length fast enough to ensure that the drifting of ϕ does not distort the shape of the LF signal so much that the QPs may not be reliably located. In the Michelson configuration considered here, one possibility to generate the optical path length sweep is to translate the reference mirror at a constant speed along the propagation axis of the reference beam.

III. INSTRUMENTATION

The scanning laser Michelson interferometer with the implemented phase-sensitive absolute amplitude detection setup is schematically shown in Fig. 3. At the detection arm, a beam splitter divides the interfering beam into two beams which are simultaneously monitored with two PDs. On one of the beam branches, a high-frequency detection circuitry, connected to the receiving port of a vector network analyzer (VNA, HP 8753E), measures the amplitude and phase of the surface vibrations at f_{vib}, and a low-speed PD records the LF signal on the other beam branch. In this setup, a separate PD is required to detect the LF signal, because the high-frequency PD (Newport 818-BB-21A) is internally ac-coupled (with 30 kHz highpass) whereas the frequency range of the LF signal is designed to be 10–100 Hz. Equally well a single dc-coupled wideband PD could be used to detect both the LF and VIB signals.

Another low-speed PD at the sample arm monitors the light power of the beam reflected back from the sample at each scan point by measuring the stray beam reflected from the $\lambda/4$ plate. The light power image provides a point-to-point correspondence with the recorded amplitude and phase data of the surface vibrations.

A linear ramp sweep of the optical path length is generated using a piezodriven reference mirror. The LF and VIB signals are recorded during the cycle when the mirror is moving toward the PBS at a constant speed. The sweep is typically set to cover at least 3 QPs (i.e., a path length change of more than $3\lambda/2$ in the reference beam) within <100 ms. The amplitude A_{vib} is calculated as an average over the amplitude values at the QPs identified from the LF data and the phase value Φ_{vib} is determined at the QP_+ point.

It should be noted that in this setup the sensitivity of the two PDs, the beam intensities of the LF and VIB branches as well as the amplifier gains of the LF and VIB signals are different. Therefore, the total optical and electrical gains of these two signal branches have been separately determined and the signal gains are compensated for before calculating the absolute amplitude from Eq. (4).

With the current detection electronics, surface vibrations can be detected in the frequency range from 30 kHz up to 2 GHz. The minimum detectable amplitude is typically ~ 1 pm with a 1 kHz intermediate frequency bandwidth of the VNA, corresponding to a measurement sensitivity of ~ 0.01 pm/$\sqrt{\mathrm{Hz}}$. The measured vibration fields have a lateral resolution of better than 1 μm, limited by the spot size of the beam focused on the sample.

IV. MEASUREMENTS

Selected measurements of two piezoactuated MEMS resonators and a fan-shaped SAW filter are presented to illustrate the performance of the detection method in the frequency range from 10 to 374 MHz. The two piezoelectrically actuated resonators are studied as potential alternatives to capacitively coupled MEMS resonators since in these structures there is no need for a bias voltage and sub-100 nm gaps. The first MEMS resonator is a square-plate resonator[13] featuring pure standing-wave vibration modes with two-valued phase data. The second sample is a beam resonator where the top metal electrode of the beam area is patterned with etched holes. It is thus a suitable sample for testing the performance of the absolute amplitude and phase detection on a surface with varying optical reflectivity. Finally, the fan-shaped SAW filter is measured to demonstrate the function of the detection scheme in the case of a propagating acoustic wave. A pure propagating wave is found between the launching interdigital transducer (IDT) and the acoustic absorber of the filter.[14]

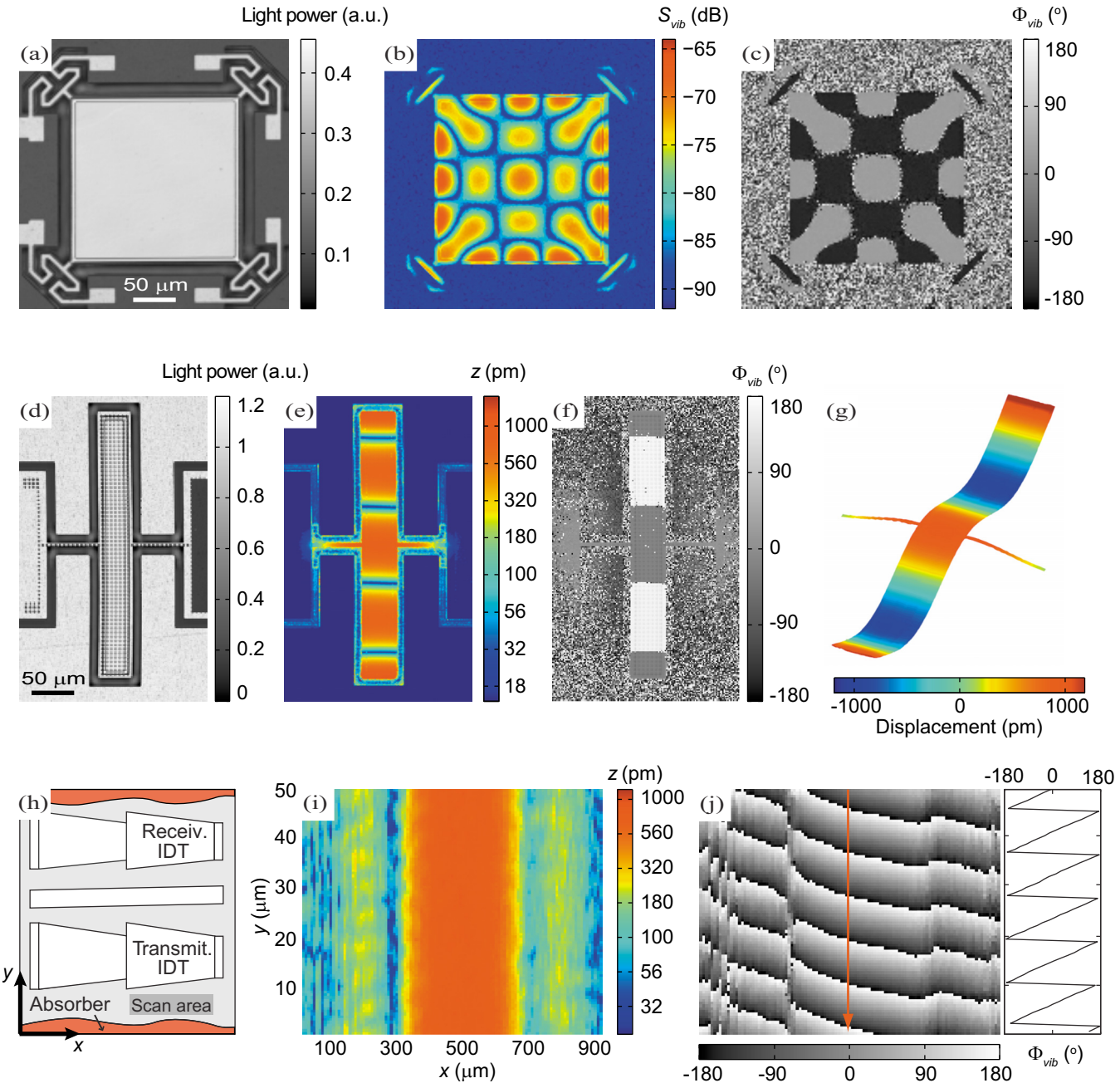

FIG. 4. (Color online) Selected measurement data of the three samples. (a) Light power image of the square-plate resonator and its (b) relative amplitude and (c) phase data at 62.0 MHz. (d) Light power image of the beam resonator and its (e) absolute amplitude and (f) phase data of the 10.1 MHz resonance mode. (g) The three-dimensional shape of the beam calculated from the amplitude and phase data of the 10.1 MHz mode at a single time instant. (h) Schematic layout of the two-track fan-shaped filter and the area scanned with the interferometer. (i) The absolute amplitude and (j) phase data at 374 MHz show a pure propagating SAW into the negative y-direction. On the right of (j), the phase of the SAW is plotted along the vertical line of the phase data indicated by the red arrow.

A. Square-plate resonator

The size of the square-plate resonator is 160 μm $\times$160 μm$\times$20 μm and it is anchored to the substrate from the corners as seen from the light power image, Fig. 4(a). The resonator features a square-extensional main vibration mode at 26.4 MHz with $Q\sim18\,000$ and a motional resistance of $R_m\sim0.24$ kΩ. The sample was driven with a nominal input power of -30 dBm (50 Ω impedance line), and it was measured in vacuum (<0.2 mbar). The scan area was 242×242 μm^2 and the scan step 1.5 μm.

In addition to the 26.4 MHz main mode, the resonator also exhibits several higher frequency modes with more complex out-of-plane vibration fields. As an example, the relative amplitude data S_{vib} (i.e., A_{vib} multiplied with the total gain of the VIB signal branch) and phase data of a 62.0 MHz mode are presented in Figs. 4(b) and 4(c). The phase data of this mode clearly show that the neighboring amplitude maxima separated by the nodes have opposite phases, which is characteristic for a standing-wave pattern.

B. Beam resonator

The main vibration mode of the beam resonator is a lateral length-extensional mode at 13.2 MHz with $Q\sim40\,000$ and $R_m\sim2.6$ kΩ. The resonator (beam area

40×320 μm^2 and thickness 20 μm) is anchored to the substrate from the center of the long sides [see Fig. 4(d)]. The beam resonator also has several other in-plane (lateral) and out-of-plane (normal to the beam surface) vibration modes. The absolute amplitude and phase data of a 10.1 MHz out-of-plane mode are illustrated in Figs. 4(e) and 4(f). The scanned area 220×356 μm^2 covers the whole resonator and some of its surroundings with a lateral scan step of 1.5 μm. The nominal input power into the sample is -30 dBm and the measurement is carried out in ambient air pressure.

The resonator is similar to that reported by Jaakkola *et al.*[15] except that certain areas of the metallization of the top surface are patterned with approximately 3 μm diameter holes. The pattern results in up to 90% variations in the optical reflectivity of the resonator surface. The measured relative amplitude data are sensitive to these reflectivity variations as they depend on the modulation depth of the interference and thus also on the intensity of the beam reflected from the sample. The absolute amplitude data, however, are expected to be insensitive to the surface reflectivity. This is due to the fact that the LF signal monitors any variations in the modulation depth of the interference, and this information is utilized when calculating the absolute amplitude using Eq. (4).

Figures 4(e) and 4(f) show that the ends of the resonator vibrate in phase with the anchors and there are additional amplitude maxima of opposite phase in between. The effects caused by reflectivity variations are negligible in the absolute amplitude data of the 10.1 MHz mode, as expected. Figure 4(g) represents the shape of the beam surface established from the amplitude and phase data at a single time instant. For illustrative purposes, a different aspect ratio in the z direction is used as the out-of-plane vibrations are more than four orders of magnitudes smaller than the lateral dimensions of the beam.

C. SAW filter

The structure of the two-track fan-shaped SAW filter is presented in Fig. 4(h). The center frequency of the filter is 374 MHz.[14] The scan area (920×50 μm^2) shown in Fig. 4(h) is located between the transmitting IDT and the bottom absorber on the right-hand-side track. The scan step is 8.36 μm along the x direction and 0.55 μm along the y direction. Ideally, a pure downward propagating SAW should exist in the scan region, if complete absorption is assumed at the absorber. A smaller scan step into the propagation direction of the SAW is used in order to obtain more detailed data of the phase fronts of the SAW. On the other hand, a resolution of 8.36 μm suffices along the x axis as the SAW field varies slowly into that direction.

The absolute amplitude and phase data of the scanned area are shown in Figs. 4(i) and 4(j). The scan was carried out in ambient air pressure with a nominal input power of 10 dBm. The data show a SAW at the center of the track that has a constant amplitude along the direction of the power flow ($-y$) and a sawtoothlike phase behavior, which is characteristic to a pure propagating wave. The vertical lineplot of the phase along the red arrow in Fig. 4(j) confirms the linear decrease in the phase (with phase wraps at -180 to 180°) to the negative y-direction of the propagating SAW. Furthermore, the normal of the phase fronts is inclined with respect to the power flow of the SAW beam which is a characteristic feature of wave motion in an anisotropic medium. Due to the unequal scan steps in x and y direction, this power flow angle appears exaggerated in Figs. 4(i) and 4(j).

V. CONCLUSION

The absolute amplitude and phase measurement method described here allows for a homodyne interferometer design without a need for active stabilization of the optical path length difference between the sample and reference beams, thus simplifying the interferometer design. The method makes an unstabilized homodyne interferometer a versatile tool for characterizing microacoustic devices as it extends the measurement capabilities of such an interferometer from relative amplitude measurements to quantitative analysis of surface vibrations. The test measurements confirm the correct functioning of the detection method. The homodyne scanning Michelson interferometer setup presented in this article enables detection of absolute amplitudes of surface vibrations up to 2 GHz with a lateral resolution of better than 1 μm and with a minimum detectable vibration amplitude of the order of 1 pm.

ACKNOWLEDGMENTS

L.L. thanks the Finnish Foundation for Technology Promotion and Helsinki University of Technology for scholarships. VTT Technical Research Centre of Finland is acknowledged for providing the MEMS samples.

[1] J. P. Monchalin, Rev. Sci. Instrum. **56**, 543 (1985).
[2] J. E. Graebner, B. P. Barber, P. L. Gammel, D. S. Greywall, and S. Gopani, Appl. Phys. Lett. **78**, 159 (2001).
[3] G. G. Fattinger and P. T. Tikka, Appl. Phys. Lett. **79**, 290 (2001).
[4] V. Annovazzi-Lodi, M. Benedetti, S. Merlo, and M. Norgia, IEEE Photon. Technol. Lett. **16**, 1703 (2004).
[5] H. Martinussen, A. Aksnes, and H. E. Engan, Opt. Express **15**, 11370 (2007).
[6] K. Kokkonen and M. Kaivola, Appl. Phys. Lett. **92**, 063502 (2008).
[7] O. Holmgren, K. Kokkonen, T. Veijola, T. Mattila, V. Kaajakari, A. Oja, J. V. Knuuttila, and M. Kaivola, J. Micromech. Microeng. **19**, 015028 (2009).
[8] R. G. White and D. C. Emmony, J. Phys. E **18**, 658 (1985).
[9] J. E. Graebner, Proc.-IEEE Ultrason. Symp. **1**, 733 (2000).
[10] J. V. Knuuttila, P. T. Tikka, and M. M. Salomaa, Opt. Lett. **25**, 613 (2000).
[11] C. B. Scruby and L. E. Drain, *Laser Ultrasonics, Techniques and Applications* (Adam Hilger, Bristol, 1990).
[12] F. Lärmer, A. Schilp, K. Funk, and C. Burrer, J. Micromech. Microeng. **6**, 177 (1996).
[13] A. Jaakkola, P. Rosenberg, S. Asmala, A. Nurmela, T. Pensala, T. Riekkinen, J. Dekker, T. Mattila, A. Alastalo, O. Holmgren, and K. Kokkonen, Proc.-IEEE Ultrason. Symp. **1**, 717 (2008).
[14] K. Kokkonen, P. Dufilie, J. V. Knuuttila, and M. M. Salomaa, Proc.-IEEE Ultrason. Symp. **2**, 1339 (2004).
[15] A. Jaakkola, P. Rosenberg, A. Nurmela, T. Pensala, T. Riekkinen, J. Dekker, T. Mattila, and A. Alastalo, Proc.-IEEE Ultrason. Symp. **1**, 1653 (2007).